Bacteriorhodopsin Enhances Efficiency of Perovskite Solar Cells

Das Subhabrata, Wu Congcong, Song Zhaoning, Hou Yuchen, Koch Rainer, Somasundaran Ponisseril, Priya Shashank, Barbiellini Bernardo, Venkatesan Renugopalakrishnan

DOI: 10.1021/acsami.9b06372

Please cite the publication as follows:

Das S., Wu C., Song Z., Hou Y., Koch R., Somasundaran P., Priya S., Barbiellini B., Venkatesan R. (2019). Bacteriorhodopsin Enhances Efficiency of Perovskite Solar Cells. ACS Applied Materials and Interfaces, Vol 11, Issue 34. p. 30728-30734. DOI: 10.1021/acsami.9b06372

Bacteriorhodopsin enhances Efficiency of Perovskite solar cells

Subhabrata Das,[‡] Congcong Wu,[¶] Zhaoning Song,[§] Yuchen Hou,[¶] Rainer Koch,["] Ponniseril Somasundaran,[‡] Shashank Priya,[*,¶] Bernardo Barbiellini,[*,⊥,#] and Renugopalakrishnan Venkatesan[*,@,O]

[‡]*Langmuir Center of Colloids and Interfaces, Columbia University in the City of New York, New York, NY 10027, USA*

[¶]*Materials Science and Engineering, Penn State, University Park, PA 16802, USA*

[§]*Department of Physics, University of Toledo, OH 43606, United States*

"*Institute of Chemistry, Carl von Ossietzky University Oldenburg, 114-118, 26129, Oldenburg, Germany*

[⊥]*Department of Physics, LUT University, FI-53851 Lappeenranta, Finland*

[#]*Department of Physics, Northeastern University, Boston, Massachusetts 02115, USA*

[@]*Department of Chemical Biology, Northeastern University, Boston, Massachusetts 02115, United States*

[O]*Department of Biophysics, Children's Hospital, Harvard Medical School, Boston, Massachusetts 02115, USA*

E-mail: sup103@psu.edu; bernardo.barbiellini@lut.fi; v.renugopalakrishnan@northeastern.edu

---

†In honor of Prof. Seeram Ramakrishna, National University of Singapore

Abstract: In recent years, halide perovskites have upstaged decades of development in solar cells by reaching power conversion efficiencies that surpasses polycrystalline silicon performance. The efficiency improvement in the perovskite cells is related to repeated recycling between photons and electron-hole pairs, reduced recombination losses and increased carrier lifetimes. Here, we demonstrate a novel approach towards enhancing the efficiency of perovskite solar cells by invoking the Forster Resonance Energy Transfer (FRET) mechanism. FRET occurs in the near-field region as bacteriorhodopsin (bR) protein and perovskite have similar optical gaps. Titanium dioxide functionalized with bR protein is shown to accelerate the electron injection from excitons produced in the perovskite layer. FRET predicts the strength and range of exciton transport between separated perovskite and bR layers. We show that the cells incorporating bR/TiO_2 layers exhibit much higher photovoltaic performance. These results open the opportunity to develop a new class of bio-perovskite solar cells with improved performance and stability.

Keywords

FRET; Purcell Effect; Photoluminescence; Fill Factor; Perovskite; Bacteriorhodopsin

1. INTRODUCTION

Organic and inorganic hybrid perovskites represent a new class of semiconductors with promising characteristics for a wide range of optoelectronic applications. Hybrid perovskites display many advantages such as long electron-hole diffusion lengths, simple fabrication procedure, sustainable chemistry, and cost-effective raw materials. Perovskites are represented by the generic formula, ABX_3, in a close-packed quasi-cubic unit cell. The A-site cations, e.g. methylammonium ($CH_3NH_3^+$) (MA), formamidinium ($HC(NH_2)_2^+$) (FA) or cesium (Cs^+)), occupy the corners of the cube; the B-site cations are typically dominated by group IVA metals with divalent oxidation state (Pb^{2+}, Sn^{2+}, Ge^{2+}); the anion X is generally a halide (Cl^-, Br^-, or I^-). In recent years, hybrid perovskite based solar cells with power conversion efficiencies up to $\geq 23\%$[1,2] have been demonstrated due to advancements in solution-synthesis and film-deposition techniques. Such an improvement has been the result of the development of new fabrication methods and the design of materials layers with proper band alignment that promotes charge transport.

In case of photovoltaic power conversion efficiency, there are several factors that contribute towards the improved performance: (1) composition-driven tunable bandgap spanning a wide range of the solar spectrum[3]; (2) direct band-gap with high absorption coefficients (high density of states above and below the band gap near the quasi-Fermi level);[4] (3) low effective masses and relatively high carrier mobilities; (4) long carrier diffusion lengths; (5) low excitonic binding energy values; (6) high photoluminescence quantum yield[5] and (7) highly efficient radiative recombination rates due to sharp band edges and absence of mid-gap states. The variation of the bandgap as a function of composition and doping level has been widely studied in hybrid perovskites. By varying cations on A and B site or anion X, a wide range of bandgaps can be achieved ranging from 1.2-2.3 eV. In typical perovskite solar cells (PSCs), several-hundred nanometer thick light absorbing layer, with or without a mesoporous scaffold, is sandwiched between the electron and hole transport layers (ETLs and HTLs, respectively). Upon the absorption of incident photons, carriers are created in the absorber that travel through a transport pathway including the ETL or HTL to the electrodes. The low non-radiative recombination rates and high photoluminescence (PL) yields of these materials allow one photo-excited state

to undergo multiple radiative emission-absorption events before it is lost through non-radiative decay. Repeated recycling between photons and electron-hole pairs creates charge extraction over large length scales, and high excitation densities within the perovskite layer allow high open-circuit voltages.[6] The architecture of PSCs is originated from the dye-sensitized solar cell (DSSC), where mesoporous TiO_2 layer is employed as a scaffold layer.[7] The high surface area of the TiO_2 mesoporous layer allows the sufficient adsorption of light absorbing molecules for energy conversion. Thavasi et al. demonstrated the feasibility of bacteriorhodopsin (bR) as bio-photosensitizer for TiO_2 in the so-called bio-sensitized solar cell (BSSC).[8] In the BSSC, bR works as a light-driven proton pump during charge separation initiated by photon absorption, with simultaneous electron ejection in the TiO_2 layer. The sensitization of TiO_2 with bR has been further rationalized by first-principles calculations performed by Koch et al.[9] and has been used by Allam et al.[10] for enhancing the photoelectrochemical water splitting.

Here we developed a new type of bio-perovskite solar cell (BPSC), as illustrated in Figure 1. The band alignment is illustrated in Figure 1a and the schematic architecture of the BPSC is displayed in Figure 1b. The valence band maximum (VBM) and conduction band maximum (CBM) for the $CH_3NH_3PbI_3$ ($MAPbI_3$) are reported to be 5.3 and 3.7 eV, respectively,[11] and the highest occupied molecular orbital (HOMO) of spiro-OMeTAD is located at 5.2 eV.[12] The favorable band alignment of perovskite with TiO_2 ETL and Spiro-OMeTAD HTL allows the charge carrier extraction to electrodes. The key component of the BPSC is the bR molecules between TiO_2 and perovskite layers, which implements the energy-transfer step involving photon absorption and hot carriers transfer. The transfer of light energy absorbed by perovskite to bR occurs first via an efficient Forster resonance energy transfer (FRET)[13,14] and further, from bR quantum dots (QD) to TiO_2, via the electron ejection mechanism of the bR proton pump mentioned above. The enhanced thermal stability of bR and its mutants, accomplished by rational site-directed mutations, provides additional advantages. The operation of these three transformative BPSC paradigms holds great promise for construction of robust and efficient electrolyte free solid-state photovoltaic devices.

2. EXPERIMENTAL SECTION

2.1 Synthesis of TiO_2/bR Layer

Cys bR mutant was immobilized on TiO_2 substrate by covalent attachment of Ti to Cys groups using standard experimental protocol.[8] The details of the synthesis and purification of bR mutants were provided in Supporting Information. bR concentration of 6.67 g/L was diluted 10 times in suspension buffer (150 mM KCl, 10 mM Tris-HCl, pH 8.2) to achieve a final absorbance of 0.2 to 0.3 at 570 nm. We mixed 0.5 mL of this diluted bR solution in suspension buffer with 250 μL of incubation buffer (300 mM KCl, 10 mM Tris-HCl, pH 7.82), and this mixture was placed on the glass substrate coated with TiO_2 incubated for 6 hr. The container was kept in the dark at room temperature during the attachment process. After 6 hr, the substrate was rinsed with incubation buffer several times, followed by drying at room temperature in the dark for 5 to 6 hr. Care was taken to keep the substrate always under dark conditions. After rinsing, visual inspection did show pink and purple spots on the TiO_2 substrates.

2.2 Perovskite Solution Preparation

The perovskite thin film was synthesized by exfoliating perovskite crystals and self-assembling to thin film.[15] To prepare the $MAPbI_3$ crystals, 1.2 M $MAPbI_3$ solution was fabricated by dissolving PbI_2 and MAI (molar ratio 1:1) in γ-butyrolactone and filtered in the vial. Next, the vial with $MAPbI_3$ solution was placed in an oil bath and slowly heated to 120 ◦C and kept for 3h for $MAPbI_3$ crystal growth. The crystals were washed with diethyl ether and dried under nitrogen gas. The $MAPbI_3$ crystals were exfoliated by exposing to methylamine CH_3NH_2 gas. The $MAPbI_3$ crystals were placed in a vial and then packed in a sealed bottle with methylamine ethanol solution for 12 h. The evaporated methylamine gas diffused into the vial and reacted with $MAPbI_3$ crystals, forming a liquid perovskite intermediate. The liquid perovskite was dissolved in acetonitrile to form 1 M perovskite solution.

2.3 Device Fabrication and Characterization

The TiO_2 compact layer was fabricated by spin-coating titanium isopropoxide (TTIP) ethanol solution on FTO glass at 2000 rpm for 20 s, followed by annealing at 500 ℃ for 1 h. To fabricate the TiO_2 mesoporous layer, the TiO_2 solution prepared by diluting 18NR-T

paste with α-terpineol and ethanol was spin-coated on the top of TiO_2 compact layer. TiO_2 layer was annealed at 500 ℃ for 1 h. The perovskite thin film was deposited by spin coating the perovskite solution onto the TiO_2 layer at 4000 rpm for 20 s and then heated at 100 ◦C for 10 min. The Spiro-OMeTAD solution was spin-coated on the perovskite layer at 4000 rpm for 20 s serving as the hole transport layer. Lastly, 80 nm of gold was thermally evaporated as the metal electrode, keeping the active area of each device at 0.096 cm^2. The steady-state and transient photoluminescence spectra were measured by FLS1000 Photoluminescence Spectrometer (Edinburgh Instruments Ltd). The samples were excited by a pulsed laser with a wavelength of 510 nm and illuminated from the film side for excitation. The Oriel Sol 3A Class AAA Solar Simulator (Newport) was employed to provide air mass (AM 1.5) illumination of 100 mW cm^{-2}. The samples were illuminated from the left (the front side) by the monochromatic (continuous) flux of photons. However, the model can be extended to an arbitrarily positioned (monochromatic or spectral) illumination source due to photon recycling and recombination events. The J-V curve was measured by Keithley digital source meter (Model 2440). The incident photon-to-current conversion efficiency (IPCE) spectra were measured by QUANTX-300 system (Newport) and the Electrochemical Impedance spectroscopy (EIS) was performed by using 600E electrochemical station (CH Instruments, Inc.).

3. RESULTS AND DISCUSSION

3.1 bR Assisted Charge Transfer

The bR molecules are integrated within perovskite solar cells by attaching on the surface of TiO_2 nanoparticles of the mesoporous layer to enhance the charge transfer between perovskite and TiO_2 ETL. Figure 2a shows the cross-sectional scanning electron microscopy (SEM) image of the BPSC, where the compact TiO_2 layer, perovskite/mesoporous TiO_2/bR, Spiro-OMeTAD, and Au electrode were deposited on the FTO glass, respectively. The thickness of perovskite and mesoporous TiO_2/bR is approximately 500 nm, which can sufficiently absorb the light. The top-view SEM of the perovskite layer deposited on TiO_2/bR was presented in Figure S1, showing a uniform, pinhole-free perovskite film with a grain size of around 200 nm. Upon light excitation, the photogenerated electrons from both capping perovskite layer and penetrated perovskite

will be transferred into the mesoporous TiO_2 by the assistance of the bR molecules. To study the coupling between bR and TiO_2, we measured the photoluminescence (PL) spectra for pristine TiO_2 film and TiO_2/bR film. The TiO_2 mesoporous film was immersed in bR solution for adsorption of bR on the surface of TiO_2 nanoparticles. As shown in Figure 2b, the pristine TiO_2 film showed no emission in the wavelength range from 600 nm to 850 nm. Upon the adsorption of bR, there is a clear emission peak around 720 nm, which can be attributed to the radiative recombination of electrons and holes excited from the bR molecules, indicating that bR is bonding on the TiO_2 surface. The absorption spectrum of the bR/TiO_2 was presented in Figure S2, showing a distinctive absorption feature of bR molecules. We then deposited $MAPbI_3$ perovskite on top of TiO_2 film and TiO_2/bR film, respectively, and measured the PL spectra, as shown in Figure 2c. The emission peak for $MAPbI_3$ is at 768 nm, corresponding to a bandgap of ~1.6 eV. Interestingly, with the adsorption of bR on TiO_2 film, the intensity of the perovskite PL decreased significantly. The effect implies that there is a charge carrier extraction at the interface between the perovskite and bR, decreasing the radiative recombination inside the perovskite and thus reducing the PL intensity. In addition, the emission peak is blue shifted from 768 nm to 762 nm, which can be attributed to the FRET with the exciton transfer from perovskite to the bR molecules. To understand the energy and charge transfer kinetics, we measured the time-resolved PL spectra to extract the charge carrier lifetime, as shown in Figure 2d. The stretched exponential PL decay can be expressed as:

$$I(t) = \sum_{i=1}^{n} I_i e^{-(\frac{t}{\tau i})^{\beta i}} \quad (1)$$

where $I(t)$ is the fluorescence intensity at time t, n is the number of components, I_i is the initial intensity of each component, τ_i is the characteristic lifetime and β_i is the stretching exponent ($0 < \beta_i \leq 1$). β deforms the exponential so that the initial decay is faster and the tail longer. The lifetime of a stretched exponential decay is quantified by its mean relaxation time $\langle\tau\rangle$:

$$\tau = \frac{\tau_c}{\beta} \int_0^{\infty} x^{(1-\beta)/\beta} e^{-x} dx \quad (2)$$

The lifetime calculated from the PL decay is τ_1= 1.31 ns, τ_2= 9.55 ns, τ_3= 24.47 ns for TiO_2/perovskite. In the case of TiO_2/bR/perovskite, the lifetime analysis yields: τ_1= 0.89 ns, τ_2= 3.63 ns, τ_3= 12.17 ns. Clearly, the lifetime of the excited electron is decreased significantly upon the adsorption of bR on TiO_2 film, which further confirms the bR can assist the charge carrier extraction from perovskite to TiO_2 ETL.

To study the effect bR molecules on the conversion efficiency of perovskite solar cells, the J-V characteristics of the two devices were measured, as shown in Figure 3a. The conventional cell (TiO_2-PSC) showed J_{sc} of 22.59 mA cm^{-2}, V_{oc} of 1.02 V, FF of 0.618, corresponding to the efficiency of 14.59%. The perovskite solar cell with bR (TiO_2/bR-PSC) exhibited J_{sc} of 22.61 mA cm^{-2}, V_{oc} of 1.05 V, FF of 0.705, with the conversion efficiency of 17.02%. The histogram of the conversion efficiency (Figure S3) shows majority devices present efficiency over 16%, and the average efficiency is 16.34%. The efficiency improvement with the bR is mainly attributed to the increased fill factor, from 0.618 to 0.705, which is due to the fast electron transfer from perovskite to bR and then TiO_2, reducing the electron transport resistance at the perovskite/TiO_2 interface. Figure 3b shows the incident-photon-to-charge conversion efficiency (IPCE) spectrum of the BPSC. The maximum external quantum efficiency (EQE) is over 95% at the wavelength of 531 nm and the EQE response edge is at around 770 nm, which is consistent with the absorption edge of $MAPbI_3$ perovskite. The integrated J_{sc} calculated from the IPCE spectrum is 22.5 mA cm^{-2}, which is consistent with the J_{sc} from J-V curve. The forward and reverse scan J-V characteristics were performed for both PSCs, as shown in Figure S4. The TiO_2-PSC exhibited a reverse-scan efficiency of 14.59% and a lower efficiency of 12.66% with forward scan. In contrast, the TiO_2/bR-PSC exhibited a reverse-scan efficiency of 17.02% and a forward-scan efficiency of 16.26%, showing a much less hysteresis, which can be ascribed to the enhanced charge transfer assisted by the bR molecules, releasing the interfacial charges at the ETL/perovskite interface. Electrochemical impedance spectroscopy (EIS) was measured to study the interfacial charge carrier transfer behavior. Figure 3c and 3d compare the Nyquist plots for the PSCs with and without bR in dark and illuminated conditions, respectively. The charge transfer resistance of the TiO_2-PSC and TiO_2/bR-PSC is 309.2 Ω and 177.5 Ω in the dark; 30.6 Ω and19.2 Ω in the 1 sun illumination condition, respectively. This reduction in the transfer resistance is attributed

to the enhanced charge extraction assisted by the bR molecules, rationalizing the increase of FF for the BPSC.

3.2 Theoretical Interpretation

The present results can be rationalized in terms of a FRET model. The lowest unoccupied molecular orbital (LUMO) and highest occupied molecular orbital (HOMO) of bR is determined by surface photo-voltage spectroscopy (SPS) to be 3.8 eV and 5.4 eV following Li et al.[16] The details of the Density Functional Theory (DFT) calculation for molecular orbitals of retinal in bR is given in the Supporting Information and the electronic transitions between the HOMO and LUMO in the retinal was illustrated in Figure S5. Since both $MAPbI_3$ and bR have almost the same gap they are resonantly coupled and FRET occurs in the near-field region. The efficiency and the spatial range of this mechanism for exciton transfer can be estimated using the near-field resonance of electric dipoles as shown by King et al.[14] The shortening of the perovskite emission lifetime upon the adsorption of bR on TiO_2 film is a clear proof that FRET provides an effective way to achieve the Purcell effect in our solar cell. [17,18] From the lifetime change, one can estimate the FRET rate as about 0.36 (1/ns). As mentioned earlier, the main effect of bR is manifested in increase in the FF of BPSC. FF is a parameter which quantifies the rectification of a solar cell device within the fourth quadrant of the J-V characteristics where power is generated. FF is influenced by charge carrier recombination losses which are significantly reduced by FRET.

In the present model shown in Figure 4a, $MAPbI_3$ replaces the semiconductor quantum dot originally considered by King et al.[14] The FRET coupling strength U is determined by the relation:

$$U = \frac{\kappa D_{Pe} D_{bR}}{s_r R^3} \tag{3}$$

where s_r is the permittivity of the medium, R is the separation between the molecules, D_{Pe} and D_{bR} are the dipole moments of the Perovskite and bR, respectively, and the angular factor κ depends on the orientations of dipoles relative to the separation between molecules. We use the dipole values of $D_{P\,e} = 1.94$ and $D_{bR} = 40$ from literature.[19, 20] We assume the medium dry and take a permittivity $s_r = 1$, $\kappa = 1$ and keep the bR-perovsite separation

distance R as a free parameter. The model also needs another parameter γ which is the inverse lifetime of an exciton in bR, and can be determined to be around 0.05 eV according to King et al.[14] Other rates can be neglected in the calculations since they are much smaller than γ. Figure 4b shows the FRET efficiency as a function of R. For separations R larger than the FRET radius R_0 the efficiency is less than 50%. Thus, in the present model, FRET radius R_0 ranges between 4-7 nm if γ varies between 0.05 and 0.1 eV. Figure 4c illustrates that for R = 2 nm, the exciton transfer from perovskite to bR occurs within a few hundred femtoseconds. Interestingly, the exciton transfer presents a damped oscillatory behavior shown by the blue curve in Figure 4c when $\gamma = 0.05$. This feature is not captured by previous FRET models and reveals that exciton transport can be coherent-like rather than diffusion-like.

4. CONCLUSION

We have developed a BPSC that utilizes novel optoelectronic characteristics of perovskite and bR. The concept of photon recycling utilized to explain the perovskite success is combined here with FRET to achieve significant improvement in the performance of PSCs. FRET is possible because of bR and perovskite possessing similar optical gaps. The perovskite acts as an antenna for photon absorption, with subsequent transfer to the retinal complex in bR. The retinal complex in bR is known to be an efficient absorber of photons through direct capture, and a similar efficiency is found for non-radiative transfer of excitons from perovskite to bR via the FRET mechanism. The decrease in photoluminescence by photosensitive bR indicates that FRET plays an important role in the excitonic transport. Thus, the present increase of FF can be explained by the fact that charge carrier recombination losses are significantly reduced by FRET process. In the future research, the nanostructure and the chemical bonding between bR and TiO_2 can be modified for enhancing the proton pumping property of bR and facilitating charge transfer, which is expected to further improve the efficiency of BPSC. This work opens a new direction to utilize the unique functionalities of biomaterials in photovoltaics for improving the charge transfer and thus the photo conversion performance.

ASSOCIATED CONTENT

Supporting Information

The procedure of synthesizing bR mutants; Top-view SEM of the perovskite layer deposited on TiO_2/bR mesoporous layer; The UV-vis absorption spectrum of bR/FTO glass by spin coating and dip coating, and the TiO_2/bR sample; Statistical power conversion efficiency (PCE) distribution of bR-incorporated PSC; Forward and reverse scan J-V characteristics of TiO_2-PSC and TiO_2/bR-PSC; Density Functional Theory (DFT) calculation for molecular orbitals of retinal in bR.

Acknowledgments

C.W. and S.P. acknowledge the support from Air Force Office of Scientific Research (AFOSR) through grant number FA9550-18-1-0233 (Biophysics and Natural Materials). We thank Kai Zhu from NREL for taking part in the fruitful discussions in the proposal of Perovskite architecture. VR thanks Wallace Coulter Foundation, Rothschild Foundation for support, Prof. Esteve Padros, Universitaria Autonoma de Barcelona, Espagna, Professor Norbert Hampp from Philipps-Universitat Marburg, Allemagne and late Prof. Har Gobind Khorana, MIT, Cambridge, MA, USA for help with Cys bR mutant.

AUTHOR INFORMATION

E-mail: sup103@psu.edu;

E-mail: bernardo.barbiellini@lut.fi;

E-mail: v.renugopalakrishnan@northeastern.edu

Notes

The authors declare no competing financial interest.

REFERENCES

(1) Etgar, L.; Gao, P.; Xue, Z.; Peng, Q.; Chandiran, A. K.; Liu, B.; Nazeeruddin, M. K.; Grätzel, M. Mesoscopic CH3NH3PbI3/TiO2 Heterojunction Solar Cells. *Journal of the American Chemical Society* **2012**, *134*, 17396–17399, PMID: 23043296.

(2) Zhao, Y.; Zhu, K. Organic–inorganic Hybrid Lead Halide Perovskites for Optoelectronic and Electronic Applications. *Chemical Society Reviews* **2016**, *45*, 655–689.

(3) Sadhanala, A.; Ahmad, S.; Zhao, K. C.; Bein, T.; Docampo, P. Blue-green color Tunable Solution Processable Organolead Chloride-Bromide Mixed Halide Perovskites for Optoelectronic Applications. *Nano letters* **2015**, *15*, 6095–6101.

(4) Lee, M. M.; Teuscher, J.; Miyasaka, T.; Murakami, T. N.; Snaith, H. J. Efficient Hybrid Solar Cells based on Meso-Superstructured Organometal Halide Perovskites. *Science* **2012**, *338*, 643–647.

(5) Tan, Z.-K.; Moghaddam, R. S.; Lai, A.; Pazos, L. M.; Credgington, D. Bright Light-Emitting Diodes based on Organometal Halide Perovskite. *Nature nanotechnology* **2014**, *9*, 687.

(6) Pazos-Outón, L. M.; Szumilo, M.; Lamboll, R.; Richter, J. M.; Crespo-Quesada, M.; Abdi-Jalebi, M.; Beeson, H. J.; Vrućinić, Photon Recycling in Lead Iodide Perovskite Solar Cells. *Science* **2016**, *351*, 1430–1433.

(7) O'regan, B.; Grätzel, M. A low-cost, High-Efficiency Solar Cell based on Dye-Sensitized Colloidal TiO2 films. *nature* **1991**, *353*, 737.

(8) Thavasi, V.; Renugopalakrishnan, V.; Jose, R.; Ramakrishna, S. Controlled Electron Injection and Transport at materials interfaces in Dye Sensitized Solar Cells. *Materials Science and Engineering: R: Reports* **2009**, *63*, 81 – 99.

(9) Koch, R.; Lipton, A. S.; Filipek, S.; Renugopalakrishnan, V. Arginine interactions with Anatase TiO2 (100) Surface and the perturbation of 49Ti NMR chemical shifts – a DFT investigation: relevance to Renu-Seeram bio solar cell. *Journal of Molecular Modeling* **2011**, *17*, 1467–1472.

(10) Allam, N. K.; Yen, C.-W.; Near, R. D.; El-Sayed, M. A. Bacteriorhodopsin/TiO 2 Nanotube arrays Hybrid system for Enhanced Photoelectrochemical Water splitting. *Energy & Environmental Science* **2011**, *4*, 2909–2914.

(11) Docampo, P.; Ball, J. M.; Darwich, M.; Eperon, G. E.; Snaith, H. J. Efficient Organometal trihalide Perovskite Planar-Heterojunction solar cells on flexible Polymer Substrates. *Nature communications* **2013**, *4*, 2761.

(12) Kim, H.-S.; Lee, C.-R.; Im, R.; Yum, J.-H.; Moser, J. E. Lead Iodide Perovskite Sensitized all-solid-state submicron thin film Mesoscopic solar cell with Efficiency exceeding 9%. *Scientific reports* **2012**, *2*, 591.

(13) Renugopalakrishnan, V.; Barbiellini, B.; King, C.; Molinari, M.; Mochalov, K.; Sukhanova, A.; Nabiev, I.; Fojan, P.; Tuller, H. L.; Chin, M.; Somasundaran, P.; Padrós, E.; Ramakrishna, S. Engineering a Robust Photovoltaic Device with Quan- tum Dots and Bacteriorhodopsin. *The Journal of Physical Chemistry C* **2014**, *118*, 16710–16717, PMID: 25383133.

(14) King, C.; Barbiellini, B.; Moser, D.; Renugopalakrishnan, V. Exactly Soluble model of Resonant Energy Transfer between molecules. *Physical Review B* **2012**, *85*, 125106.

(15) Wu, C.; Li, H.; Yan, Y.; Chi, B.; Pu, J.; Li, J.; Sanghadasa, M.; Priya, S. Cost- effective sustainable-engineering of CH3NH3PbI3 Perovskite Solar Cells through slicing and restacking of 2D layers. *Nano Energy* **2017**, *36*, 295–302.

(16) Li, L. S.; Xu, T.; Zhang, Y. J.; Jin, J.; Li, T. J.; Zou, B.; Wang, J.-P. Photovoltaic characteristics of BR/p-silicon Heterostructures using Surface Photovoltage Spectroscopy. *Journal of Vacuum Science & Technology A: Vacuum, Surfaces, and Films* **2001**, *19*, 1037–1041.

(17) Pelton, M. Modified Spontaneous Emission in Nanophotonic Structures. *Nature Photonics* **2015**, *9*, 427.

(18) Barbiellini, B.; Das, S.; Renugopalakrishnan, V.; Somasundaran, P. Electromagnetic Field in Hybrid Quantum Plasmonic-Photonic Systems. *Condensed Matter* **2018**, *3*, 10.

(19) Senanayak, S. P.; Yang, B.; Thomas, B.; Goedel, K.; Guha, S.; Moya, X. Understanding Charge Transport in Lead Iodide Perovskite thin-film Field-effect Transistorsransistors. *Science advances* **2017**, *3*, e1601935.

(20) Kietis, B.; Macernis, M.; Sulskus, J.; Valkunas, L. Estimation of the Permanent Dipole moment of Bacteriorhodopsin. *Lithuanian Journal of Physics* **2010**, *50* .

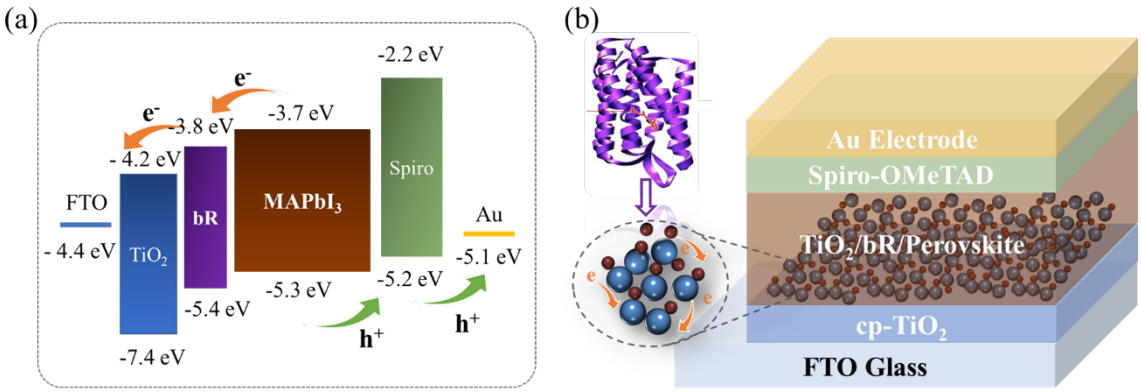

Figure 1. (a) Band alignment of the bR/perovskite solar cell (BPSC). (b) Schematic of the BPSC architecture, where the compact TiO_2 layer, perovskite/mesoporous TiO_2/bR, Spiro-OMeTAD, and Au electrode were deposited on the FTO glass, respectively.

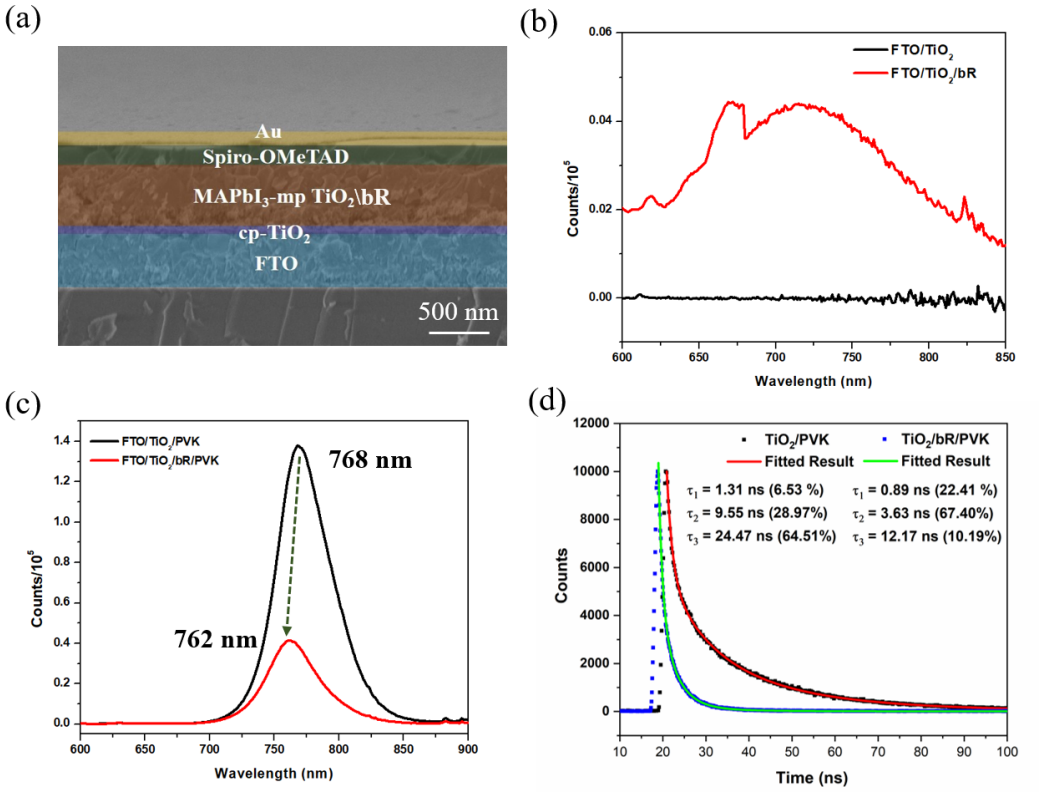

Figure 2. (a) Cross-sectional SEM of BPSC. (b) Steady-state photoluminescence (PL) spectra of TiO_2 and TiO_2/bR layers. (c) Steady-state and (d) time-resolved PL spectra TiO_2/perovskite layer and TiO_2/bR/perovskite layer.

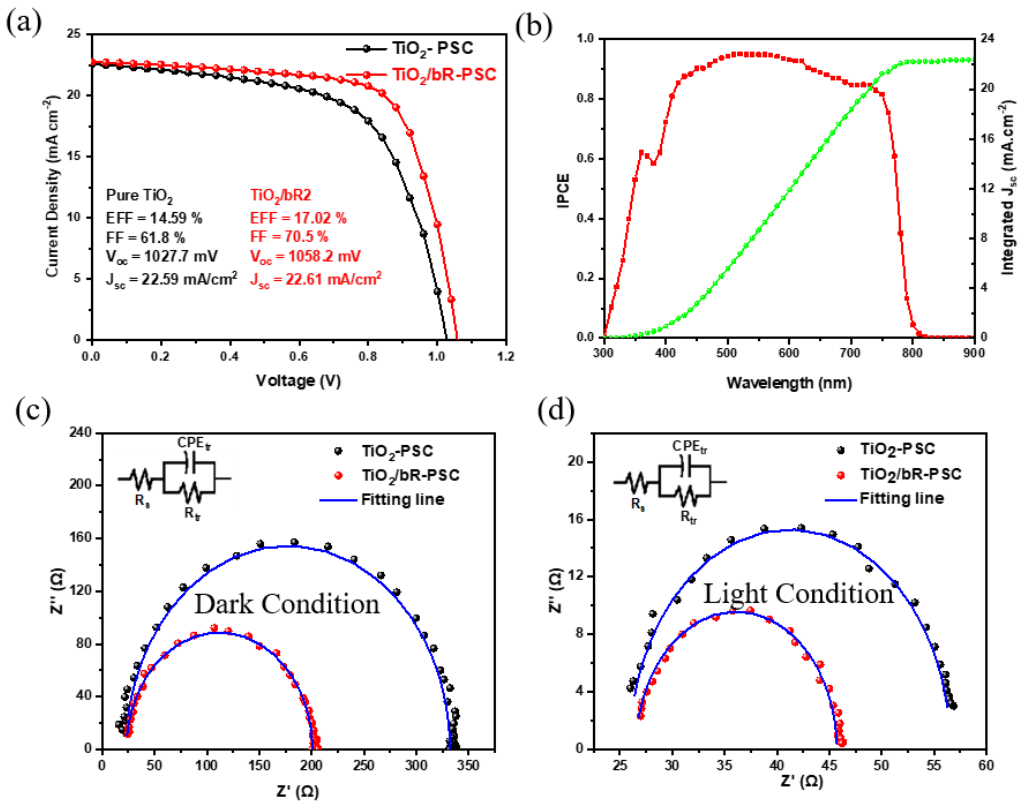

Figure 3. (a) J-V characteristics of the perovskite solar cell with and without bR integration. (b) IPCE and the integrated J_{sc} of the BPSC. EIS of the PSCs with and without bR in the (c) dark and (d) illumination conditions.

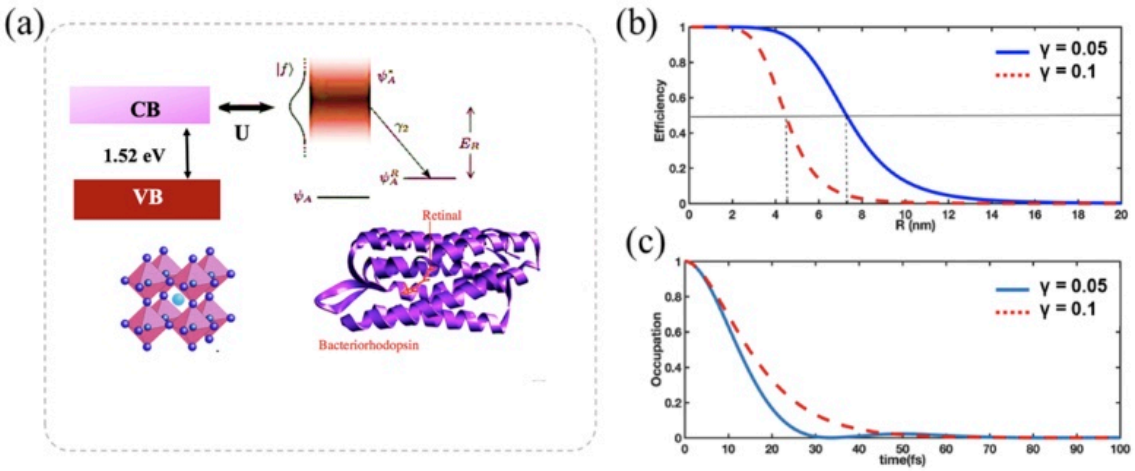

Figure 4. (a) Schematics of FRET model showing perovskite interaction with bR. (b) Exciton transport efficiency for bR-perovskite as a function of separation. (c) Occupation probability of initial excited state for R=2 nm as a function of time for $\gamma = 0.05$ and 0.1 eV.